Monthly Notices
of the
ROYAL ASTRONOMICAL SOCIETY

MNRAS **484,** 3078–3092 (2019) doi:10.1093/mnras/stz108

The central star of planetary nebula PHR 1315 − 6555 and its host Galactic open cluster AL 1

V. Fragkou,[1,2]★ Q. A. Parker,[1,2]★ A. Zijlstra,[3] R. Shaw[4] and F. Lykou[1,2]

[1]*Department of Physics, The University of Hong Kong, Pok Fu Lam Road, Hong Kong SAR, China*
[2]*Laboratory for Space Research, The University of Hong Kong, Pok Fu Lam Road, Hong Kong SAR, China*
[3]*Jodrell Bank Centre for Astrophysics, School of Physics and Astronomy, University of Manchester, M13 9PL, UK*
[4]*TScI at the Steven Muller Building, 3700 San Martin Drive, Baltimore, MD 21218, USA*

Accepted 2019 January 9. Received 2019 January 9; in original form 2018 October 5

ABSTRACT

PHR 1315 − 6555 is a rare case of a Galactic planetary nebula that is a proven member of the open cluster AL 1. This membership allows its distance to be defined with precision, and thus accurate measurements of its physical characteristics along with the parameters of its central star (CS) can be obtained. In this work, we use the *Hubble Space Telescope* to detect this unique CS and constrain the cluster's physical parameters. Our results suggest that the cluster is at a distance of ∼12 kpc, is highly reddened, and has an age of about 0.66 Gyr and a turn-off mass of ∼2.2 $M_{\odot}$. Our deep colour–magnitude diagram suggests that the metallicity of the cluster is subsolar ($Z = 0.006$). Our photometric measurements indicate that the planetary nebula's core is a faint blue star close to the nebular apparent centre, with an observed dereddened visual VEGA magnitude of 21.82 ± 0.60. A significant contribution from any possible binary companion is unlikely but possible. Our results show that the CS has an effective Zanstra temperature of about 113 kK and a mass of 0.58 $M_{\odot}$, providing a unique additional point in the fundamental white dwarf initial-to-final-mass relationship.

Key words: planetary nebulae: individual: PHR 1315 − 6565, Andrews–Lindsay 1.

1 INTRODUCTION

At the end of their lives, low-to-intermediate-mass stars (∼1 to ∼8 $M_{\odot}$) pass through the asymptotic giant branch (AGB) phase. At this point they lose most of their mass, and if their remnant stellar cores reach temperatures high enough to ionize the ejected material, a planetary nebula (PN) is formed around them. These central stars of planetary nebulae (CSPNe) evolve at constant luminosities towards higher effective temperatures. After their fuel is exhausted they will eventually cool along the white dwarf (WD) cooling track. Their evolution depends on the thermal pulse cycle phase during which the star left the AGB phase (Schönberner 1983; Vassiliadis & Wood 1994; Blocker 1995).

Because the AGB mass loss is mainly dust-driven (Wood 1979; Bowen 1988) and the formation of the dust depends strongly on metallicity, high-metallicity AGB stars lose a larger amount of matter than do stars of lower metallicities (Willson 2000) and consequently result in less-massive CSPNe (see Villaver, Stanghellini & Shaw 2003; Villaver, Stanghellini & Shaw 2004). Furthermore, in the case of mass loss under a lack of dust, low-metallicity AGB stars are physically smaller for a given luminosity and mass (Willson, Bowen & Struck 1996; Willson 2000), and as a result their mass-loss rates are reduced (see Villaver et al. 2004). This dependence of mass-loss rates has as a consequence that in low-metallicity environments and for a given initial stellar population, more main sequence (MS) stars reach the Chandrasekhar limit and produce Type II supernovae (see Villaver et al. 2004).

PNe are visible for only a short time period (∼10 000–30 000 yr, Badenes, Maoz & Ciardullo 2015) before their ionized material dissipates. Their evolutionary time-scales depend on the progenitor masses of their CSPNe (e.g. Villaver, Manchado & García-Segura 2002). CSPN masses are crucial for understanding post-AGB evolution because they provide additional data for the widely used WD initial-to-final mass relationship (IFMR; e.g. Ferrario et al. 2005; Dobbie et al. 2009; Kalirai et al. 2008) and information about the dredge-up efficiency during the AGB phase (see Parker et al. 2011; Moreno-Ibáñez et al. 2016). A reliable IFMR is a powerful tool when using WD luminosity functions to estimate the age of the Galactic disc and of open clusters using field WDs and cluster WD populations respectively. They can help us to trace the enhancement of both nitrogen and carbon in entire galaxies (see Parker et al. 2011). The IFMR has some correlation with metallicity (Weidemann 1987; Vassiliadis & Wood 1994; Marigo & Girardi 2007; Miller Bertolami 2016), because the upper mass limit for WD production is lower in metal-poor environments (see Villaver

★ E-mail: vfrag@physics.auth.gr (VF); quentinp@hku.hk (QAP)

et al. 2003). Moreover, the mass loss and the convection mechanisms constrain the upper limits for the initial mass of stars that will evolve into WDs (Blocker 1995; Herwig 2000). Neither of these processes, however, is well understood. Thus any precise measurements of CSPN and WD masses are of major importance (see e.g. Villaver et al. 2003).

The initial mass of a CSPN can also drive the chemistry of the resulting PN, because higher-mass progenitors tend to form PNe with enhanced N, which are usually of axisymmetric or bipolar morphologies (Type I PNe, Peimbert 1978; Peimbert & Torres-Peimbert 1983). This is corroborated by the fact that Galactic bipolar PNe tend to be found at low Galactic latitudes (Corradi & Schwarz 1995; Manchado et al. 2000; Stanghellini et al. 2002; Parker et al. 2006). From the hydrodynamic modelling of such massive progenitor stars (e.g. Villaver et al. 2002; Perinotto et al. 2004), we expect Type I PNe to be optically thick (e.g. Kaler & Jacoby 1989) for the majority of their lifespans. In some cases they may never turn into optically thin nebulae, although bipolar PNe may be optically thin in their lobes and thick in the torus (see Moreno-Ibánez et al. 2016). As a result, PN morphologies can provide clues regarding the physical properties of the PNe themselves (e.g. Stanghellini, Shaw & Villaver 2016).

Despite their importance for stellar evolution, CSPN studies are difficult because the inherent luminosities of these objects are low and they are often too faint to be easily detected compared with the surrounding nebula (Shaw & Kaler 1985). Measurements of their masses and other characteristics require a precise (accuracy better than 10 per cent, Shaw 2006) determination of their distances (see Villaver, Stanghellini & Shaw 2007). Although the accurately known distances of external galaxies allow the study of their PNe, and in some cases their CSPNe (e.g. Villaver et al. 2003; Villaver et al. 2004), such a task is extremely difficult for PNe in our Galaxy because only a few Galactic PN distances have been determined with sufficient precision (see Moreno-Ibánez et al. 2016). Precise parallax measurements currently exist for only a very small fraction (sigma/parallax $= \sigma/\pi \sim 5$ per cent, Benedict et al. 2009) of nearby Galactic PNe, and large statistical uncertainties (∼20–30 per cent, Stanghellini, Shaw & Villaver 2008; Giammanco et al. 2011; Frew, Parker & Bojičić 2016) affect the distance estimates of bulk PNe (see Majaess et al. 2014), although this situation is likely to change in the near future, at least for nearby PNe, with the complete data release from the GAIA mission (Gaia Collaboration et al. 2016).

PNe that are members of Galactic stellar clusters have the advantage that an accurate (< 10 per cent) determination of their distances can be made from cluster colour–magnitude diagrams (CMDs), and precise measurements of their physical properties such as age, physical dimensions, chemical composition (as this can be considered idependently from the host cluster's metallicity), effective temperature and mass of the progenitor star can be made from fits to cluster isochrones (Parker et al. 2011; Turner et al. 2011; Moni Bidin et al. 2014). Furthermore, photometric measurements of their CSPNe can constrain their intrinsic luminosity and mass, and thus these objects can be used as additional points for the IFMR (Parker et al. 2011).

Unfortunately, evolved stars going through the PN phase in open clusters are very hard to find. This is because open clusters usually survive for less than 1 Gyr (Bonatto & Bica 2011), so by the time the dominant low-mass stars enter the PN stage the cluster will have completely dissipated. Clusters with longer lifespans are generally more massive and so can host greater numbers of massive stars. However, the more massive of these stars do not evolve as PNe (e.g. Majaess, Turner & Lane 2007). The lifetimes of PNe from progenitor stars of a few solar masses in young clusters are short, only about 10^3–10^4 yr (see Majaess et al. 2014), making their detection unlikely. Hence, any examples uncovered are rare jewels for scientific exploitation. Until now, only five PNe have been found to be physically associated with stellar clusters in our Galaxy. Four are in extremely long-lived globular clusters (Pease 1928; Gillett et al. 1989; Jacoby et al. 1997). So far, only one (PHR 1315 − 6555) has been proven to be a member of an intermediate-age open cluster (OC hereafter, Parker et al. 2011), with a turn-off (TO) mass of $\sim 2.2\,M_\odot$.

PHR 1315 − 6555 is a faint bipolar, probably Type I, PN, discovered through the AAO/UKST SuperCOSMOS Hα survey (Parker et al. 2005), whose radial velocity, interstellar extinction and statistical distance measurements show that it is a member of the distant Galactic OC Andrews–Lindsay 1 (AL 1). It has an apparent angular diameter of 80 arcsec (Parker et al. 2011; Majaess et al. 2014).

The cluster isochrone-derived distance for this PN of 10 kpc has been estimated to be the most accurate currently determined for a PN in our Galaxy (sigma/distance $= \sigma/d = 4$ per cent, Majaess et al. 2014), and although this puts it beyond the reach of *GAIA* (Gaia Collaboration et al. 2016), it allows the direct study of the CSPN.

In this work we present our deep *Hubble Space Telescope* (*HST*) F555W and F814W photometry of the cluster, the PN and its CSPN. This has allowed us to create an improved CMD of the cluster, to explore the nebular microstructure and to determine the physical properties of its CSPN, a unique and rare addition for the WD IFMR. In Section 2 we investigate the physical properties of the OC AL 1, while in Section 3 we examine the PN and its CSPN. Finally, in Section 4 we discuss our results and in Section 5 we present our conclusions.

2 THE OPEN CLUSTER ANDREWS–LINDSAY 1

AL 1 is a distant and faint compact OC that lies close to the solar circle (see Carraro, Vallenari & Ortolani 1995) and was first detected by Andrews & Lindsay (1967) and van den Bergh & Hagen (1975). Its ESO Schmidt plates designation is ESO 96-SC04 (Lauberts 1982), and a number of authors have explored its properties (Phelps, Janes & Montgomery 1994; Janes & Phelps 1994; Carraro at al. 1995; Carraro & Munari 2004; Frinchaboy et al. 2004a,b; Carraro, Janes & Eastman 2005; Majaess et al. 2014).

Janes & Phelps (1994) found a distance of 7.5 kpc to the cluster using the mean luminosity of its red giant clump, but considering the cluster's sparseness this is probably an underestimation of its true distance (Carraro et al. 1995). Using the photometric data from Phelps et al. (1994) for the calibration of their frames, Carraro et al. (1995) found that the best fit of their B and V observed magnitudes of 2059 cluster stars on the Padova isochrone scales (Girardi et al. 2000) predicts a cluster age of 0.7 Gyr and a reddening $E(B-V) \sim 0.75$ mag. This agrees within the errors with the value obtained by Neckel & Klare (1980) for the visual absorption in the direction of the cluster ($A_V = 1.7$–1.9 mag). Although their dereddened TO colour $(B-V)_0$ indicates that the cluster's metallicity (Z) is probably slightly lower than solar (also supported from abundance measurements of [Fe/H], which was found to be -0.51 ± 0.3 by Frinchaboy et al. 2004a), the isochrones of $Z = 0.008$ do not fit their data. Thus, assuming solar metallicity, they derived a distance to the cluster of about 11.8 kpc. This leads to cluster Galactic coordinates of $X = -9.6$ kpc, $Y = 1.7$ kpc and $Z = -0.7$ kpc (Carraro et al. 1995).

Table 1. The physical parameters of AL 1 as determined in this work and by previous authors.

Distance [kpc]	$E(B-V)$	Age [Gyr]	Reference
12 ± 0.5	0.83 ± 0.05	0.66 ± 0.10	This work
10 ± 0.4	0.72	0.794 ± 0.106	Majaess et al. (2014)
16.95	0.34 ± 0.05	0.8 ± 0.2	Carraro et al. (2005)
12 ± 1	0.7 ± 0.2	0.8	Carraro & Munari (2004)
9.35	–	0.67	Frinchaboy et al. (2004b)
11.8	0.75	0.7	Carraro et al. (1995)
7.57	0.72	–	Janes & Phelps (1994)

Carraro & Munari (2004) collected *BVI* photometric data for 890 cluster stars and, also assuming a solar metallicity, found a cluster age of 0.8 Gyr, a distance of 12 ± 1 kpc and a reddening of 0.7 ± 0.2 mag, in close agreement with the results of Carraro et al. (1995). Their results indicate that the progenitor mass of PHR 1315 − 6555 is about 2.5 $M_{\odot}$ (e.g. Girardi et al. 2000), weakly depending on Z, while Majaess et al. (2014) estimated a TO mass for the cluster of 2.3 $M_{\odot}$.

The cluster physical parameters derived by the different authors are summarized for convenience in Table 1. Their large spread reflects the difficulty of studying a faint and distant cluster suffering from large contamination from field stars (see Majaess et al. 2014). The more disparate results by Carraro et al. (2005) were undertaken under poor weather conditions. In the following, we present our new calculations for the parameters of this faint cluster using our deep *HST* F555W and F814W photometry. The results have enabled us to obtain an improved CMD, which extends 4 to 5 mag fainter than any CMD previously obtained for this particular cluster.

2.1 Observations and data reduction

Under Program ID: 12518 (2012 March 6), we obtained both long and short time exposures in each of the *HST* WFC3 (Wide-Field-Camera 3, Kimble et al. 2008) F555W and F814W filters, centred on the cluster's apparent centre (see Fig. 1). We did this in order to cover the full dynamic range of the cluster stars with a signal-to-noise ratio (S/N) $\geq$ 30 from above the red giant clump ($V \sim 16$) to the faint end of the cluster's luminosity function ($V \sim 26$). These two filters measure the V and I continuum respectively, and have passbands very similar to those of the Johnson–Cousins system. Because the WFC3 field of view (162 arcsec × 162 arcsec) is nearly identical to the size of the cluster, these observations allow the construction of a CMD that samples the entire cluster effectively. The complete observing log can be seen in Table 2.

The pixel size of the UVIS channel of WFC3 is 0.04 arcsec per pixel (Dressel 2012), and observations were made with a gain of 1.5 e^{-}/ADU. The images were processed using the standard WFC3 calibration pipeline (CALWFC3 version 3.4.1, 2017 April 10; the full calibration process is described in Rajan et al. 2011).

The IRAF/DAOPHOT package was used to analyse our data and to measure the magnitudes of the cluster stars (Stetson 1987; Davis 1994). DAOPHOT requires an initial estimate of the full width at half-maximum (FWHM), and thus we obtained a FWHM estimate of about 4 pixels for the stellar profiles of our long exposures and of about 2.8 for our short exposures. We identified the stars in our images, measured their instrumental magnitudes, and calculated and fitted a point spread function (PSF). We considered the fraction of the stellar PSF that falls outside the measured stellar apertures to perform aperture correction. We finally transformed the measured values to the Space Telescope magnitude system (STMAG), which is based on a spectrum with constant flux per unit wavelength, following Dressel (2017). Because the WFC3/UVIS channel presents a variable PSF (Sabbi & Bellini 2013), about 20–30 bright and relatively isolated stars spread around each image were used for its calculation. The detailed processing steps of IRAF/DAOPHOT are described in Artusi et al. (2016). The zero-point calibration (= −21.10 as provided by *HST*) for the transformation to ST magnitudes is described in Koornneef et al. (1986) and Horne (1988).

We checked our data for consistency by comparing our measured F555W magnitudes with the visual magnitudes measured for the same stars by Majaess et al. (2014). Fig. 2 shows that our magnitudes agree with those previously measured for the cluster stars, taking into account the difference in the magnitude systems used. The apparent scatter can be explained by the fact that lower-resolution ground-based observational data are more affected by blending in a crowded field, such as the one studied here. Finally, we excluded saturated stars in our images and removed duplications for magnitudes obtained from both our short and long exposures in both filters. Our measured magnitudes were then transformed into the VEGA magnitude system VEGAMAG using the corresponding zero points provided by the *HST* WFC3 handbook (Rajan et al. 2011).

2.2 Constraining the physical parameters of AL 1

A deep F555W − F814W versus F555W CMD was constructed for AL 1 using our derived F555W and F814W VEGA magnitudes for 5118 stars in our field of view (Fig. 3). The cluster lies at a low Galactic latitude and as a result suffers from high interstellar extinction and strong contamination by field stars (see Carraro et al. 1995). This is evident from our CMD and makes recognition of the cluster's TO point difficult.

For this reason, the Bayesian field star decontamination algorithm from the ASTECA code (Perren, Vázquez & Piatti 2015) was used. After rejecting stars with magnitudes that have very large errors, it uses photometric data to determine the cluster's radial density profile and radius and assigns cluster membership probabilities (for a complete description of the code, see Perren et al. 2015). The cluster's centre was located at about RA = $13^{h}15^{m}16^{s}$ and Dec. = $-65^{\circ}55'16''$, and its radius was estimated to be 57 arcsec. The code provided 1180 stars with membership probabilities larger than 50 per cent, which were consequently used for the construction of a CMD decontaminated from the majority of field stars (Fig. 4).

The main features of our new improved cluster CMD can now easily be seen. The TO point is located at about F555W = 18.6 VEGAMAG and F555W − F814W = 1.12, while the MS ends at about F555W = 18.1 VEGAMAG and F555W − F814W = 1.09.

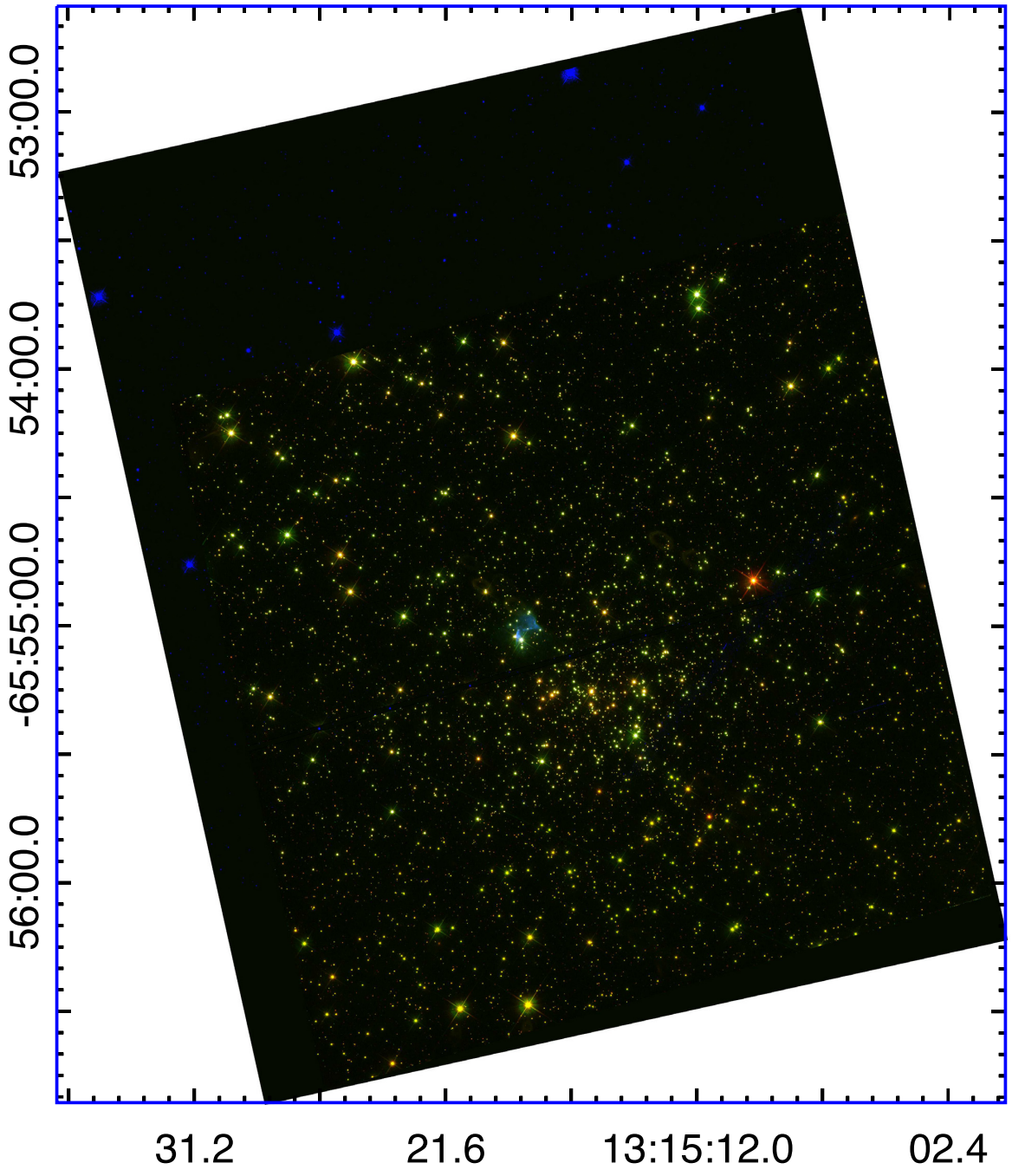

Figure 1. A colour composite image of our *HST* field of view of the open cluster AL 1. The F502N narrow-filter image is blue, the F555W long-exposure image is green, and the F814W long-exposure image is red. Colours have been adjusted in each Red-Green-Blue (RGB) channel to try to represent the natural star colours.

The red giant clump can be seen between F555W $=$ 17.6 and 18.0 VEGAMAG.

Although the ASTECA code can also be used for deriving a cluster's physical parameters, it is not reliable for relatively young clusters that suffer from strong field contamination (Perren et al. 2015), as is the case here. Because the brightest stars in our field are saturated, there is a lack of evolved stars in our data. As such, we decided not to use the ASTECA code for this purpose. Instead, as a starting point for the cluster's age derivation, the age index ΔV was used, as described by Carraro & Chiosi (1994), which is defined as

Table 2. Imaging log for *HST* program ID: 12518.

α [h m s]	δ [° ′ ″]	Exposure time [s]	Filter	λ_c [Å]
13:15:18.90	−65:55:01.00	1000	F502N	5009.60
13:15:16.00	−65:55:16.00	1020	F555W	5305.95
...	...	1020	F5814W	8048.10
...	...	1020	F200LP	4939.20
...	...	1100	F350LP	5871.50
...	...	36	F555W	5305.50
...	...	40	F814W	8043.70

HST observing log for the field on 2012 March 6.

the difference between the V magnitude of the red clump and 0.25 mag below the end of the MS. The age index ΔV is then linked to the age (τ) of a cluster as

$$\log(\tau_{\rm Gyr}) = 0.45(\pm0.04) \times \Delta V + 8.58(\pm0.23) \quad (1)$$

(Carraro & Chiosi 1994, their equation 3). In our case and using the mean magnitude of the red clump (F555W $= 17.8$), the age index is about 0.55, which translates to an age of $0.68\ ^{+0.54}_{-0.30}$ Gyr, which is in good agreement with previous estimates (see Table 1). The age spread is given from the terms in parentheses in equation (1) because it is larger than the error induced by the red clump spread.

The reddening estimation was made by visual fitting of our CMD to theoretical Padova isochrones (Girardi et al. 2000; Bressan et al. 2012; Chen et al. 2015) for the ages close to that derived above and with different metallicities (see Fig. 4). A best-fitting isochrone is found for a metallicity of $Z = 0.006$, an age of 0.66 Gyr and a colour excess of $E(B-V) \approx 0.83 \pm 0.05$ ($A_V = 2.57 \pm 0.16$, using the extinction laws by Cardelli, Clayton & Mathis 1989 and $R_V = 3.1$) that reproduces the main features of our data (see Fig. 5). From this reddening value and the location of the TO point we derive a distance modulus $(m-M) = 15.4 \pm 0.1$, which translates into a cluster distance of 12 ± 0.5 kpc. Among the results from previous authors (see Table 1), this distance is consistent only with the distance values given by Carraro et al. (1995) and Carraro & Munari (2004). The errors reflect the visual fitting of the theoretical isochrone (the maximum error is the point where it is clear that the theoretical isochrone no longer fits our data). The constrained physical parameters for AL 1 imply a TO mass for the cluster stars of about 2.2 $M_\odot$.

3 THE BIPOLAR PLANETARY NEBULA PHR 1315 − 6555 AND ITS CSPN

One of the main motivations for our *HST* observations was to obtain a clear identification of the CSPN, which was not possible from our previous data. The sensitivity and spatial resolution of *HST* enable the detection and measurement of the faint CSPN of PHR 1315 − 6555 against its background nebula in the crowded field of AL 1 for the first time.

3.1 Observations and analysis

Our long F555W and F814W exposures allow the faint CSPN to be resolved and the determination of its V- and I-band continua. The effect of binarity has been proposed as a possible explanation for the formation of bipolar PNe (De Marco 2009) as it is clear from the *HST* imagery that PHR 1315 − 6555 is a bipolar PN. Our deep F814W-band exposure was thus carefully examined to investigate the possibility of a cool companion.

Additional *HST* exposures were obtained with the narrow-band [O III] WFC3 F502N filter to show the PN in finer detail. These yielded a signal-to-noise ratio of about 10 per resolution element. The long-pass F200LP and F350LP filters give a signal-to-noise ratio of about 20 for a CSPN with the expected properties. The F200LP filter collects light of all wavelengths where the detectors are sensitive, presenting a remarkable sensitivity at near-ultraviolet (near-UV) wavelengths (Dressel 2017), while the F350LP filter passes all visible light blocking the UV. As a consequence, the difference of its calibrated flux from those of F200LP gives the near-UV continuum (see Moreno-Ibánez et al. 2016). The F502N-filter exposure reveals the nebular microstructure (Fig. 6), confirming its bipolar morphology, while the UV continuum ensures that the ionizing CSPN will be correctly identified because it is expected to be the brightest in this bandpass. The images have been processed as described in Section 2.1.

3.2 The physical parameters of PHR 1315 − 6555

This unique PN, in terms of its confirmed location in a Galactic OC with accurately known distance and progenitor mass, is located only 23 arcsec from the cluster centre. It was previously reported that it has an ionized mass of 0.5 $M_\odot$ (Parker et al. 2011), although in this work we found a smaller value (see below). Furthermore, its optical image indicates that it is evolved and probably optically thick (Parker et al. 2011). The presence of a strong He II 4686-Å emission line shows that it is a high-excitation nebula. The crossover (Ambartsumyan) method (Kaler & Jacoby 1989) predicts a CS apparent visual magnitude of 23.5 ± 1 and an effective temperature of 20.9×10^4 K (Parker et al. 2011). The calculated PN excitation class parameter, Exp $= 9.8$ (Reid & Parker 2010), predicts an even higher CS effective temperature, of about 26.5×10^4 K, but such high CS temperatures are not expected for such evolved PNe (Parker et al. 2011 estimated a PN age of about 11 000 yr), and a temperature of 10×10^4–14×10^4 K and CS mass of about 0.6–0.65 $M_\odot$ seem more reasonable (Parker et al. 2011).

Adjusting the contrast in the [O III] narrow-band image (see Fig. 6, top right), the full extent of the nebula is revealed, allowing measurement of its apparent diameter. The nebula has two main lobes with a NW–SE-oriented waist, with some faint emission on its SE side. Drawing two axes, along the nebular waist (length 4.48 arcsec) and lobes, we estimate the nebular apparent diameter as the length of its major axis of 14.3 arcsec. An adopted distance of 12 ± 0.5 kpc results in a PN physical diameter of 0.83 ± 0.04 pc.

3.3 Identifying the CSPN of PHR 1315 − 6555

In order to identify our CSPN, the F200LP and F350LP filter exposures were used, because their subtraction can reveal the bluest star in the nebular field. Using the IRAF/DAOPHOT package (Stetson 1987; Davis 1994) and the same procedures as above for the determination of the F200LP and F350LP VEGA magnitudes (see Section 3.1), a F200LP − F350LP versus F200LP CMD of all unsaturated stars in our field of view was constructed for locating the expected F200LP − F350LP colour of the relatively blue stars in our field. The $Z = 0.006$ subsolar Padova theoretical isochrone for the cluster parameters derived in the previous section was fitted to our data (Fig. 7) to locate the MS. The small shift of our data to the red can be explained by their mean F200LP − F350LP error

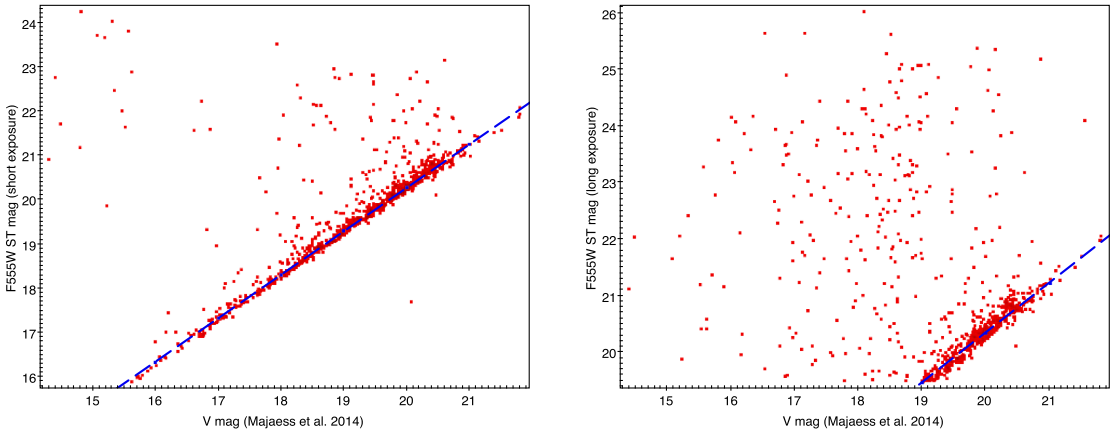

Figure 2. Comparison of our measured F555W short-exposure (left panel) and long-exposure (right panel) magnitudes with the *V* magnitudes from Majaess et al. (2014). The apparent scatter is due to star blending issues caused by the relatively low resolution of ground-based observations towards a crowded field. Because the conversion of the *HST* F555W filter depends on the spectral energy distribution of each star, a least-squares fitting routine was applied to both the short and long *HST* exposures. After the removal of outliers, the solutions are visualized with the blue tracks. Both fits are very similar: our short-exposure data give a solution of F555W $= 0.98V + 0.68$, while the long-exposure data give a solution of F555W $= 0.88V + 2.75$. Because our short-exposure data have a better overlap with the data of Majaess et al. (2014), we expect the solution from our short-exposure data to better represent the relationship between the different filters.

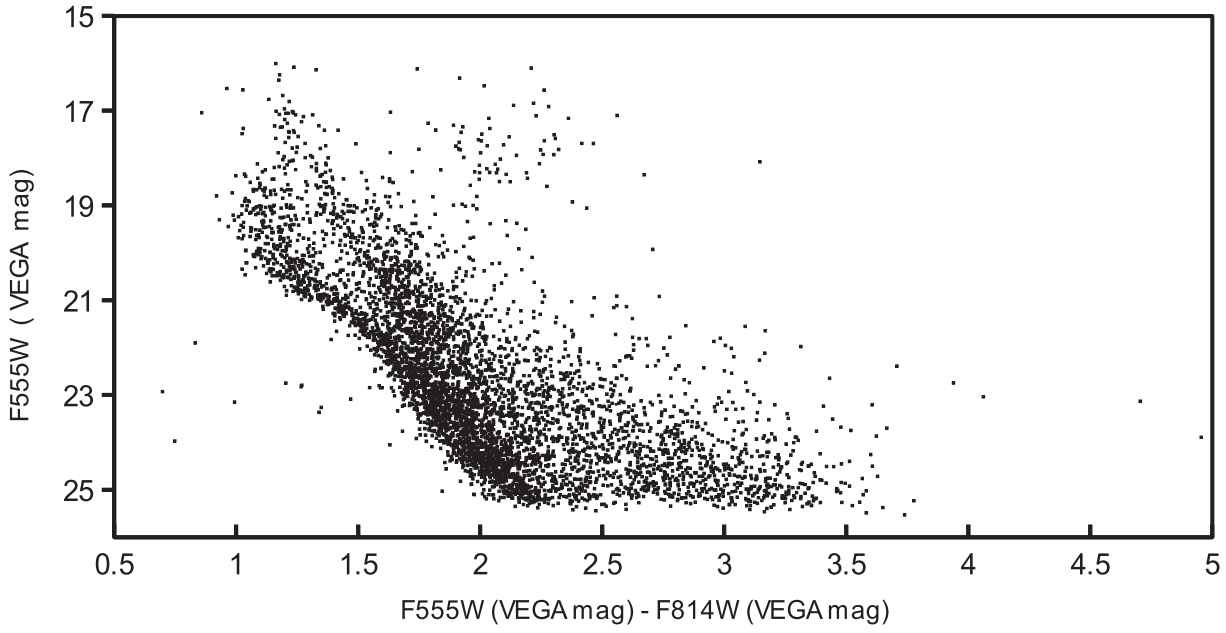

Figure 3. The AL 1 cluster F555W − F814W versus F555W colour–magnitude diagram from the measured VEGA magnitudes of all (non-saturated) stars in our *HST* field of view. The main sequence of the cluster can been seen as a tight locus to the left, distinct from that of the field stars.

of 0.068. All blue stars in the field, including our CSPN, should be located to the left of the MS.

Only six stars in the nebular field lie blue-wards of the MS (towards smaller F200LP − F350LP colours, see Fig. 7); they are indicated by circles in the F555W flux-calibrated long-exposure nebular image (Fig. 8). The star that is located closest (just south) of the centre of the nebular waist shows a reddened F200LP − F350LP = 0.32 ± 0.08, indicating that it is actually relatively red and thus cannot be our CS. Because the bluest star in the field with RA $13^{h}15^{m}18^{s}.72$ and Dec. $-65^{\circ}55'01''.16$ (circled in red in Fig. 8) lies only 1.46 arcsec from the centre of the nebular waist (which has an apparent diameter of 4.48 arcsec and is also indicated in Fig. 8), we are confident that this is the true CSPN.

3.3.1 *Aperture photometry*

The newly identified CSPN F555W, F814E, F200LP and F350LP VEGA magnitudes were measured by aperture photometry using the IRAF/PHOT task (Davis 1989). For the nebular subtraction we decided not to use our monochromatic [O III] image, because this approach induces large errors in the derived CSPN magnitudes. Instead, after determining the stellar radial profiles, we measured the flux

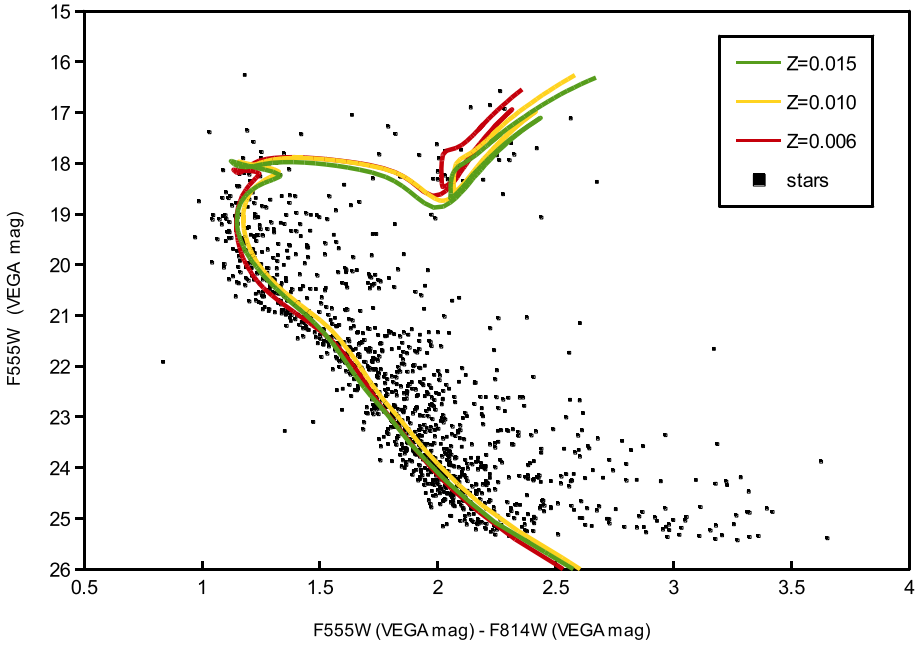

Figure 4. Padova theoretical isochrones for various metallicities fitted to our F555W − F814W versus F555W colour–magnitude diagram after decontamination from field stars. The mean F555W and F555W − F814W errors of our stellar data are 0.08 and 0.09 respectively. The parameters that produced each isochrone are, for $Z = 0.015$, age $= 0.66$ Gyr, $E(B - V) = 0.77$, distance modulus $= 15.6$; for $Z = 0.01$, age $= 0.66$ Gyr, $E(B - V) = 0.82$, distance modulus $= 15.4$; and for $Z = 0.006$, age $= 0.66$ Gyr, $E(B - V) = 0.83$, distance modulus $= 15.4$.

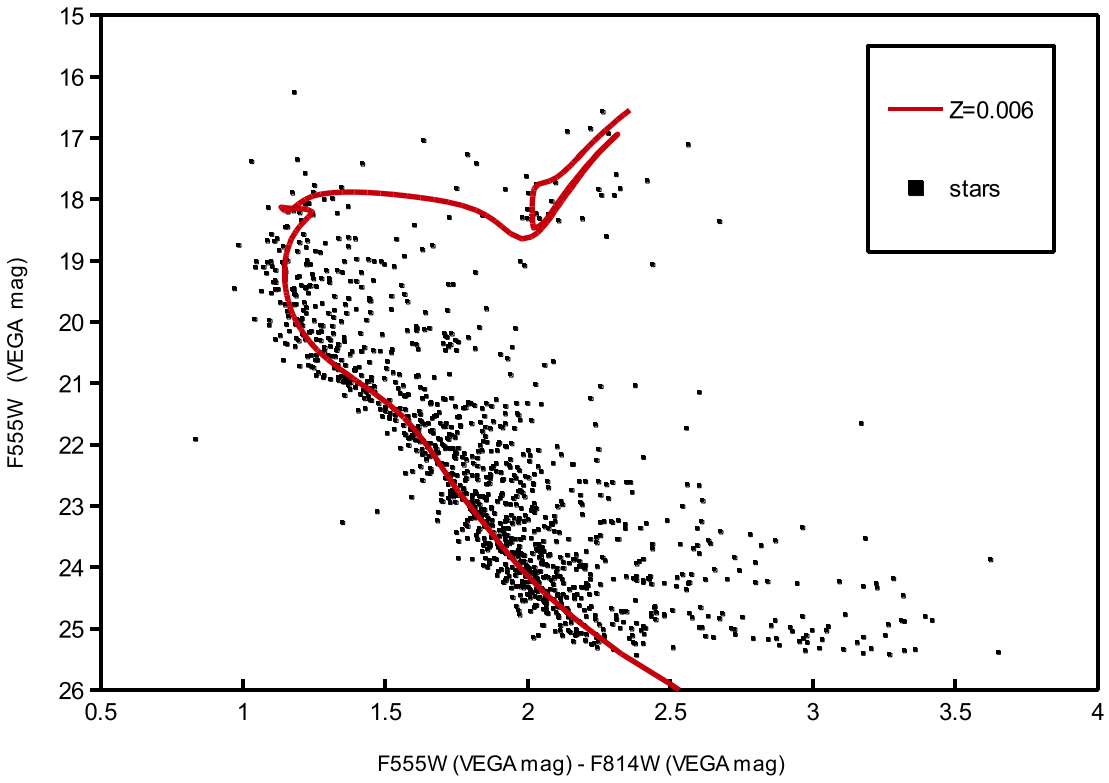

Figure 5. The best-fitting Padova theoretical isochrone fitted to our F555W − F814W versus F555W colour–magnitude diagram. The adopted parameters are as in Fig. 4 for $Z = 0.006$.

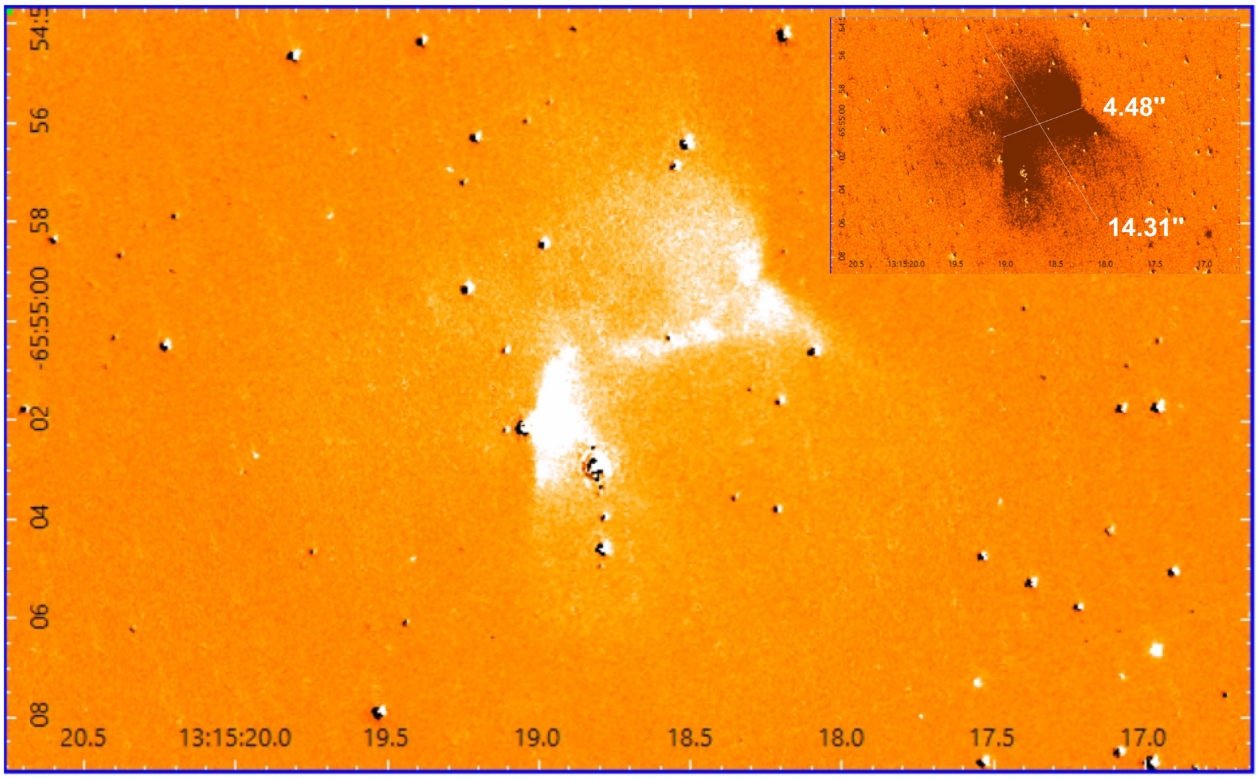

Figure 6. The visual continuum (F555W)-subtracted, flux-calibrated [O III] (F502N) nebular image. North is at the top, east is on the left. The full extent of the clearly bipolar nebula can been seen in the top right, adjusting the contrast on the main image.

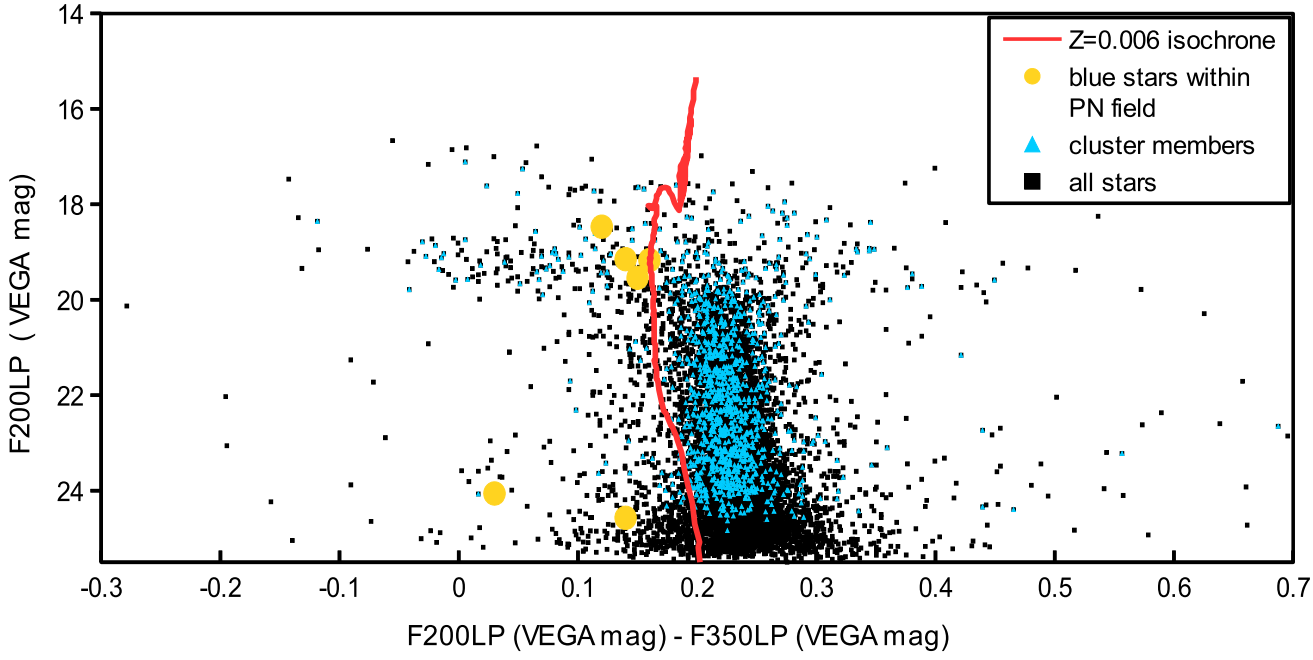

Figure 7. A subsolar Padova theoretical isochrone for the cluster parameters derived earlier fitted to our F200LP − F350LP versus F200LP colour–magnitude diagram from the measured VEGA magnitudes of all unsaturated stars in our field of view. The small shift of our data to the red can be explained by their mean F200LP − F350LP error of 0.068. The blue triangles indicate the cluster members as derived before by the decontamination algorithm from the ASTECA code (Perren et al. 2015). The yellow circles indicate the six stars within the nebular field that lie blue-wards of the main sequence.

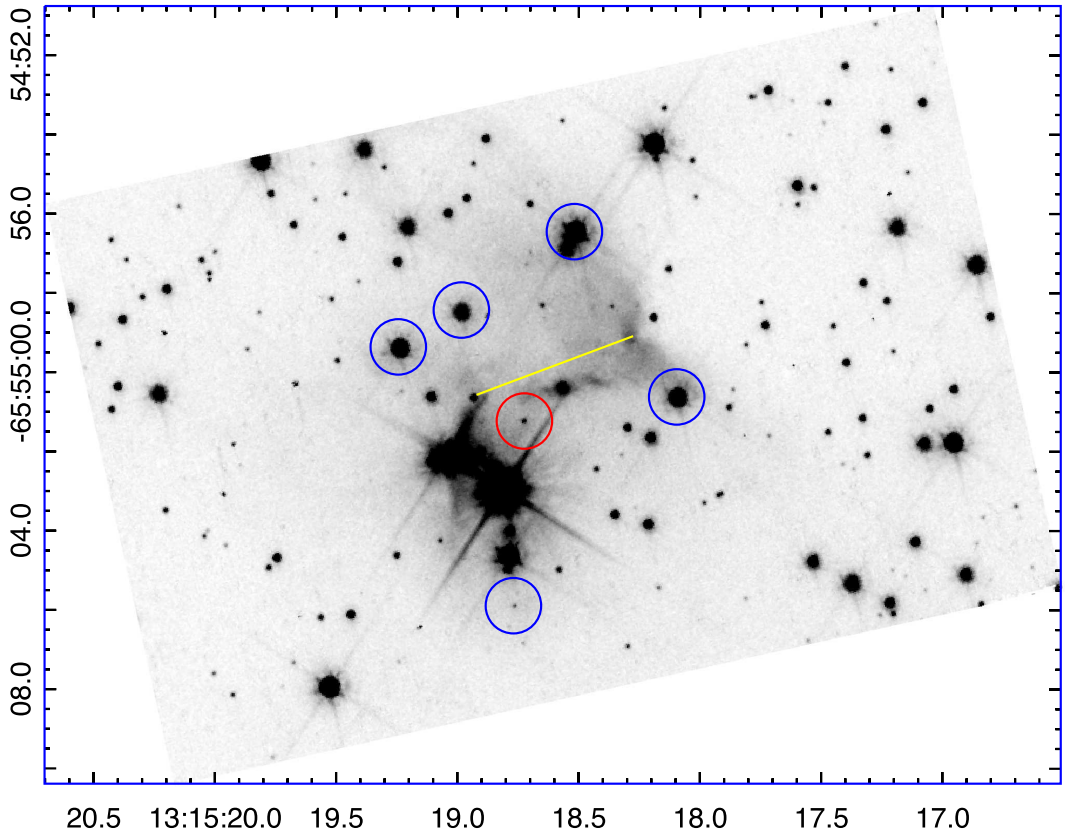

Figure 8. The F555W flux-calibrated long-exposure nebular image. The blue stars are indicated by circles. The bluest star of all in the nebular field lies only 1.46 arcsec from the centre of the nebular waist and is circled in red. The yellow line indicates the nebular waist, which has an apparent diameter of 4.48 arcsec. North is at the top, east is on the left.

inside a circular aperture around the stars' centre, subtracting the background and nebular contribution by selecting an annulus close enough to the selected apertures to sample it. The selected width of the sky annulus of 3 pixels (just outside our 4-pixel aperture) ensures that the nebular continuum will be suitably subtracted. This approach may affect our photometric measurements because some small portion of the stellar PSF may fall outside our selected apertures. We consider the effect negligible, as the background will be still dominated by the nebular flux (see Moreno-Ibánez et al. 2016).

The measured stellar fluxes were then transformed to ST and then to VEGA magnitudes (see Section 2.1). Uncertainties reflect the systematic errors in the flux derivation, such as the deviation of the rms of the background about its median value and the Poisson uncertainty in the flux measurements (see Moreno-Ibánez et al. 2016).

3.3.2 *Extinction correction*

No internal nebular extinction could be measured from the spectral data of Parker et al. (2011), as is usually the case for such evolved and faint PNe. Interstellar extinction uncertainties are rarely a problem at optical wavelengths when the flux calibration is accurate, as in their work. In the following, we assume that there is no nebular internal extinction present. We corrected our magnitudes for interstellar extinction following Kaler & Lutz (1985) and using the $E(B-V) = 0.83 \pm 0.05$ reddening value derived above (see Section 2.2), which agrees with the PN reddening that Parker et al. (2011) found from the Balmer decrement ($E(B-V) = 0.83 \pm 0.08$). The adopted reddening value affects the transformation of our measured VEGA magnitudes to the standard Johnson–Cousins system and may lead to a larger error (Moreno-Ibánez et al. 2016). The resulting dereddened F555W, F814W, F200LP and F350LP VEGA magnitudes are presented in Table 3.

3.3.3 *Transformation of derived VEGA magnitudes to the Johnson–Cousins magnitude system*

Our derived F555W VEGA magnitude may not be adequate for calculating the effective temperature and luminosity of our CSPN, and transformation to the standard Johnson–Cousins system is essential. The transformation depends on the SED of our object. A blackbody spectrum can be regarded as a good approximation

Table 3. The extinction-corrected F555W, F814W, F200LP, F350LP and Johnson *V* and *I* VEGA magnitudes of our CSPN, as measured by aperture photometry, along with their errors.

Filter	VEGAMAG
F555W	21.90 ± 0.60
F814W	22.65 ± 0.75
F200LP	20.73 ± 0.37
F350LP	21.46 ± 0.36
V	21.82 ± 0.60
I	22.65 ± 0.75

for representing the SEDs of CSPNe (Gabler, Kudritzki & Mendez 1991).

Following the same steps as in Moreno-Ibánez et al. (2016), the required colour was estimated by synthetic photometry using the IRAF/STSDAS SYNPHOT package, which assumes a blackbody spectrum for representing an object's SED and calculates the difference in the magnitude between the two systems (for a complete guide to the SYNPHOT package, see Laidler et al. 2005). For the calculation of our CSPN's Johnson *V* and *I* magnitudes, we used our derived F555W and F814W VEGA magnitudes respectively, because the passbands of these two *HST* filters are the most similar to those of the standard *V* and *I* magnitudes. Because we do not know the CS effective temperature in advance, we calculated its *V* − F555W difference taking the median of colours derived assuming blackbody spectra of effective temperatures between 30 000 and 300 000 K in steps of 5000 K, adding their standard deviation quadratically to the errors of the derived Johnson magnitudes. The lower limit used for the effective temperature of a CSPN is the lower temperature required for the production of adequate ionizing photons to form a PN, while the upper limit is the higher CSPN temperature suggested by the Vassiliadis & Wood (1994) evolutionary tracks.

After estimating the effective temperature of our CSPN from the He II nebular emission line flux (see Section 3.3.4) and the derived *V* magnitude, we repeated our transformation calculations using this fixed temperature, recalculated the *V* magnitude, and iterated this process until convergence was reached (derived effective temperature variations less than 10 K and stable transformation colour). The final derived effective temperatures were also used for the transformation of our measured F814W to the Johnson *I* VEGAMAG. The calculated final standard *V* and *I* VEGAMAG along with their errors are also presented in Table 3.

3.3.4 *Zanstra temperatures*

The CSPN effective temperature has been calculated in PYNEB (Luridiana, Morisset & Shaw 2015) via the well-known Zanstra method, described by Zanstra (1931) and developed by Harman & Seaton (1966) and Kaler (1983). The Zanstra technique assumes that the nebula absorbs all photons above the Lyman limit of H ($\lambda < 921$ Å) or He^+ ($\lambda > 228$ Å). A comparison of the flux of the H I or He II nebular recombination line with that of the stellar visual continuum enables the star's total ionizing flux to be determined. Each recombination gives a Balmer series photon as it is usually the case at high optical depth. The error of the CSPN temperatures obtained via this method is usually less than 30 per cent (see Gleizes, Acker & Stenholm 1989) and is affected by the uncertainties in the measured fluxes (see Tylenda et al. 1989).

Table 4. The derived physical properties of our CSPN.

Property	Unit	Value
T_H Zanstra estimate	(10^3 K)	69.03 ± 10.35
T_{He} Zanstra estimate	(10^3 K)	112.68 ± 16.90
TR		1.63
Bolometric correction (BC)	(from T_H)	− 5.44 ± 0.45
	(from T_{He})	− 6.90 ± 0.45
$\log(L/L_\odot)$	(from T_H)	1.51 ± 0.30
	(from T_{He})	2.09 ± 0.30
$M/M_\odot$ (derived from VW tracks)	(from T_H)	< 0.50
	(from T_{He})	$0.62^{+0.12}_{-0.09}$
$M/M_\odot$ (derived from MBM tracks)	(from T_H)	< 0.50
	(from T_{He})	$0.58^{+0.14}_{-0.08}$

Under the so-called Zanstra discrepancy (see e.g. Gruenwald & Viegas 2002), the temperatures derived with this method from the He II line (T_{He}) are usually higher and more accurate than those derived from the H I line (T_H). For optically thin PNe, T_H generally underestimates the true CSPN effective temperature. For high-temperature values, the nebula is optically thick to the H ionizing radiation, and their ratio (TR) approaches unity (e.g. Kaler 1983; Kaler & Jacoby 1989; Gruenwald & Viegas 2000). Because the CSPN temperature at which the nebular transition from optically thick to thin occurs is directly related to the progenitor's mass, a high Zanstra discrepancy usually implies a low-mass progenitor (Villaver et al. 2002). In our case, the presence of He I in the PN spectrum indicates that the nebula is optically thick, while that of He II implies a high CSPN temperature (see Moreno-Ibánez 2016), so a derived (T_H) should be considered a fairly good approximation to the true temperature value. However, the Zanstra temperature derived from the He II line is preferred for the derivation of candidate CSPN luminosities and masses as an even better approximation to their actual temperatures (see e.g. Villaver et al. 2003, 2004; Moreno-Ibáñez et al. 2016). We need to note the possibility of a nebula becoming optically thin to He II at particularly high stellar temperatures (Shaw & Kaler 1989), in which case the Zanstra temperatures derived in this way should be considered as lower limits (see e.g. Villaver et al. 2003).

Using the H I and He II nebular spectral flux measurements by Parker et al. (2011), corrected for interstellar extinction (see Section 3.3.2) using the reddening value derived above, and our measured extinction-corrected stellar visual magnitude, we calculated both the H I and He II Zanstra temperatures, which are presented along their ratio (TR) and errors in Table 4. The temperature errors reflect uncertainties of 15 per cent (see Preite-Martinez & Pottasch 1983).

3.3.5 *Luminosities*

With the assumption that the Zanstra temperatures are good approximations for the CSPN effective temperature, we now calculate the bolometric correction factor (BC) using

$$BC = 27.66 - 6.84 \log T_{\rm eff} \quad (2)$$

(Vacca, Garmany & Shull 1996), where for $T_{\rm eff}$ we used our derived T_H and T_{He}. This relationship only weakly depends on a star's surface gravity. It assumes a $T_{\rm eff}$ of not more than 50 000 K (Vacca et al. 1996; Flower 1996), but considering that there are no other

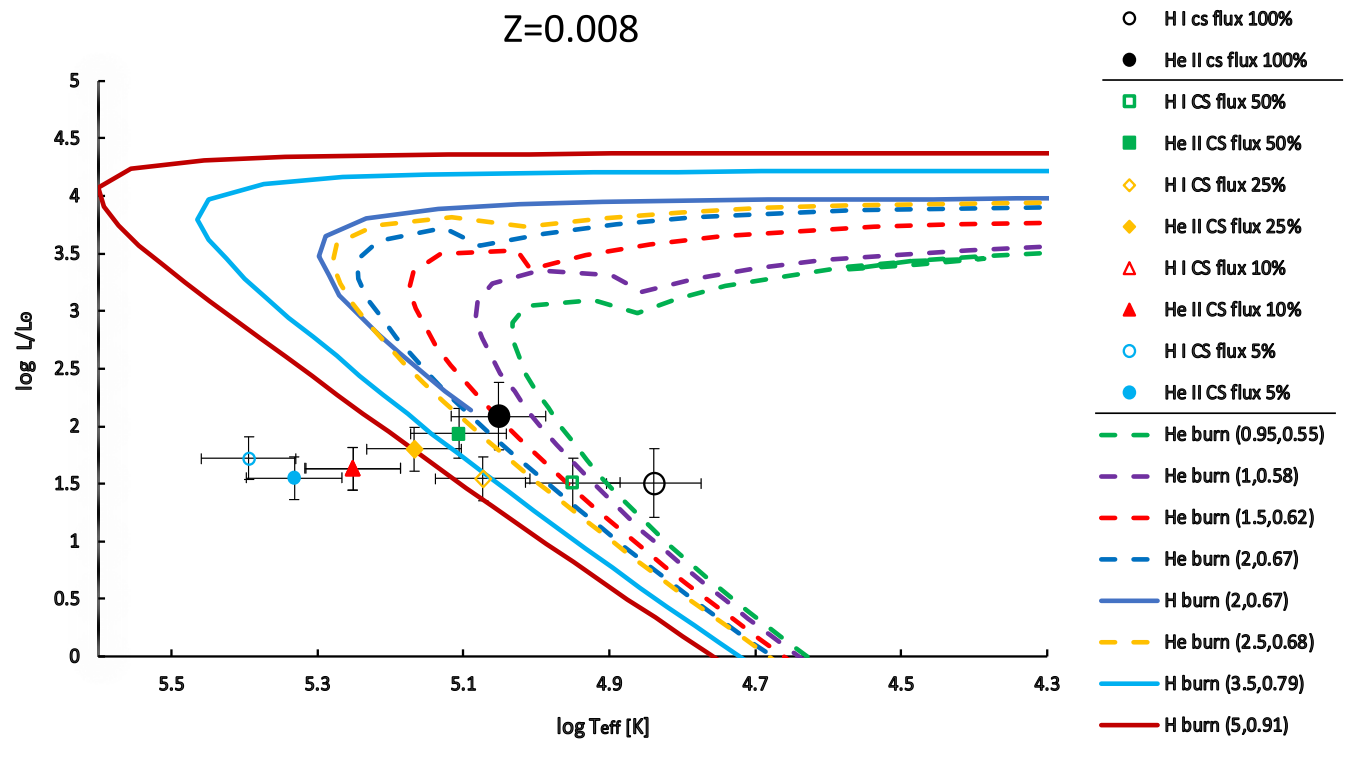

(a)

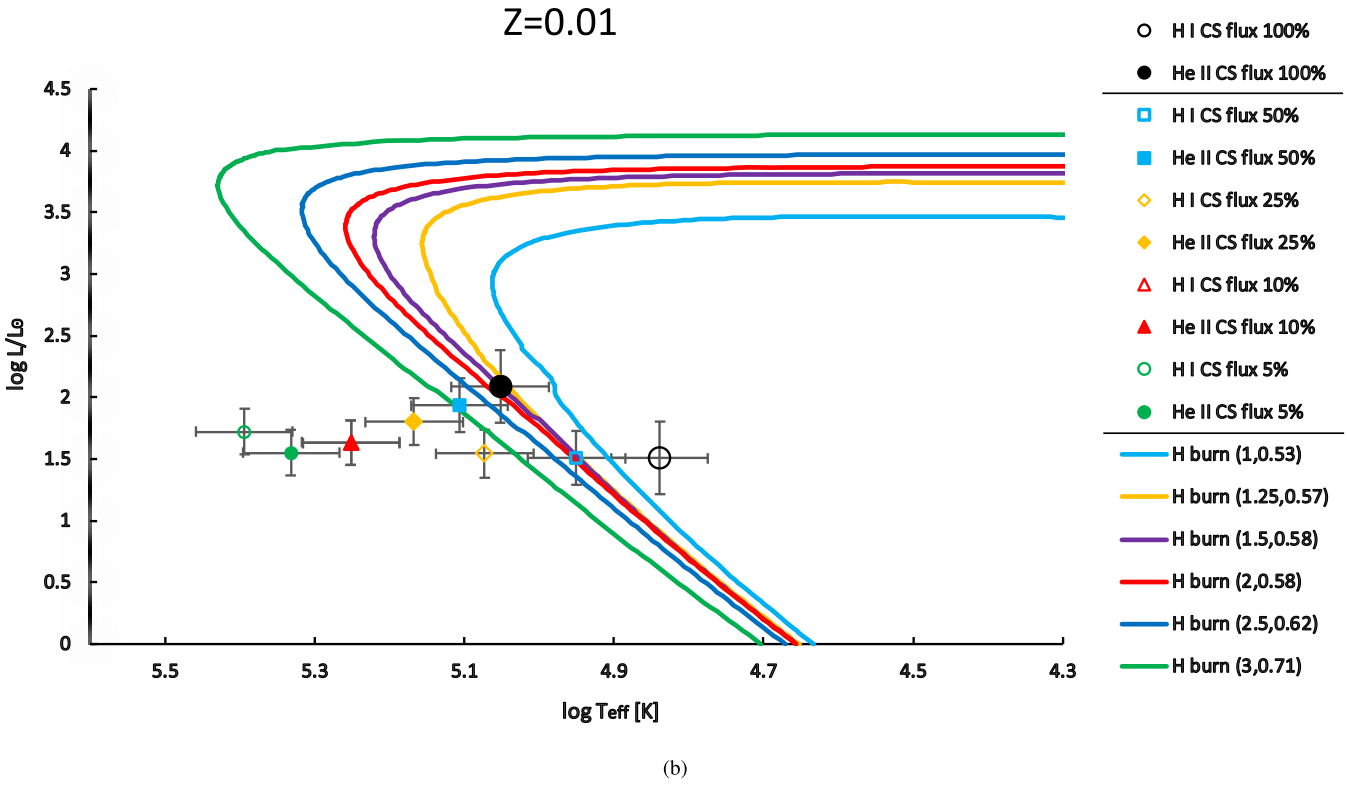

(b)

Figure 9. The computed physical parameters of our CSPN for various companion flux contributions plotted along with the VW $Z = 0.008$ (upper panel) and MBM $Z = 0.01$ (lower panel) evolutionary tracks. Open and full points represent the central star luminosities and temperatures calculated from Zanstra temperatures that were derived from the H I and He II planetary nebula emission lines respectively. The legend for the evolutionary tracks indicates the initial and final masses that produced them.

Table 5. Derived parameters assuming different contributions from a binary companion.

Companion star			CSPN					
Contribution [%]	M [$M_\odot$]	Spectral type	V^a [VEGAMAG]	T_H [10^3 K]	T_{He} [10^3 K]	$\log(L/L_\odot)^b$	VW M^c [$M_\odot$]	MBM M^d [$M_\odot$]
50	0.66	K7V	22.65 ± 0.33	89.15 ± 13.37	127.77 ± 19.17	1.94 ± 0.22	$0.73^{+0.17}_{-0.13}$	0.71 ± 0.14
75	0.71	K5V	22.21 ± 0.46	118.38 ± 17.76	147.06 ± 22.06	1.80 ± 0.19	$0.91^{+0.17}_{-0.19}$	–
90	0.74	K5V	22.01 ± 0.54	178.39 ± 26.76	178.47 ± 26.77	1.63 ± 0.18	–	–
95	0.74	K5V	21.95 ± 0.57	247.91 ± 37.19	214.61 ± 32.19	1.55 ± 0.18	–	–

Notes. [a]Corrected for interstellar extinction.
[b]Derived from T_{He}.
[c]Derived from T_{He} and VW tracks.
[d]Derived from T_{He} and MBM tracks.

Table 6. Derived data on any IR excess of our CSPN. Quoted magnitudes are in the VEGA magnitude system VEGAMAG and are uncorrected for interstellar extinction.

Property	Value
T_{He} [10^3 K]	112.68 ± 16.90
F555W	24.47 ± 0.58
F814W	23.89 ± 0.75
F250LP	24.28 ± 0.33
F350LP	24.19 ± 0.33
$(F555W - F814W)_{mod}$	0.749
$\Delta_{obs-mod}$(F555W − F814W)	-0.174 ± 0.665
$(F200LP - F350LP)_{mod}$	0.016
$\Delta_{obs-mod}$(F200LP − F350LP)	0.067 ± 0.463

calibrations in the literature suitable for hot stars we assume the derived values to be valid for our purposes (see Moreno-Ibánez et al. 2016).

The known PN distance allows the calculation of the absolute luminosity of our CSPN. Adopting a value of 15.4 for the distance modulus (see Section 2.2), we can estimate the CSPN absolute visual magnitude M_v (= 6.42), and adding the BC found previously we derive its luminosity L as

$$L = -\frac{M_{V(bol)} - M_{\odot(bol)}}{2.5} \log(L/L_\odot), \quad (3)$$

where $M_{\odot(bol)} = 4.75$ mag (Allen 1976). The derived BC and luminosity are shown in Table 4, where their errors have been computed through standard error propagation.

3.3.6 *CSPN masses*

The presence of the He II line in a PN's emission spectrum implies effective temperatures higher than 50×10^3 K (Osterbrock & Ferland 2006). The effective temperature derived here from the H I line is lower than that predicted from the nebular spectral measurements (Parker et al. 2011), indicating that the nebula is optically thin relative to H I. The temperature derived from the He II line is also lower than what the PN's spectral data suggest (high He II/Hβ line ratio) but is consistent with what is expected for an optically thick PN so it better represents our data.

We determined the CSPN H I and He II masses by plotting the derived luminosities and temperatures in the log$T$–log$L$ plane along with the Vassiliadis & Wood (1994, from now on VW tracks) and latest Miller Bertolami (2016, from now on MBM tracks) post-AGB evolutionary tracks for single stars and assume subsolar metallicities close to the cluster metallicity derived above ($Z = 0.008$ for VW tracks and $Z = 0.01$ for MBM tracks), as shown in Fig. 9. VW evolutionary tracks are plotted for both H-burning and He-burning post-AGB stars, whose nature depends on the dominant burning shell at the time they leave the AGB phase. The He-burning tracks are more accurate for low-mass progenitors (Vassiliadis & Wood 1994), but because He-burning CSPNe account for only ∼25 per cent of the total CSPN population (e.g. Iben 1984; Wood & Faulkner 1986; Schönberner 1986; Renzini 1989) and we account for an intermediate-mass progenitor of about 2 $M_\odot$ (see Section 2.2), we derive the stellar masses (see Table 4) using only their H-burning tracks when possible (note that for the adopted metallicity, VW H-burning trucks are not available for relatively low-mass stars).

The CSPN masses from both the VW and the MBM tracks were calculated by interpolating the values obtained from the closest tracks plotted, with the errors reflecting the uncertainties in the luminosities and temperatures. They are presented in Table 4. Both sets of tracks represent our data well within the errors.

3.4 Investigating the possibility of a stellar companion

CSPN luminosities, effective temperatures and masses were calculated assuming the lack of a binary companion. This assumption is rather precarious, however, particularly for a bipolar PN because complex PN shapes are believed to be the result of binary systems (De Marco 2009; De Marco et al. 2013; García-Segura et al. 2014). The presence of a companion would imply that the derived effective temperatures and masses are only lower limits (Kaler 1983).

In order to explore the possibility of an unresolved companion contributing to our measured visual flux, we follow the procedure in Villaver et al. (2004) and assume that different fractions of the flux come from a hypothetical stellar companion. We considered companion contributions to the total measured visual fluxes between 50 per cent and 95 per cent, because a smaller fraction is not expected to significantly change the CSPN mass estimates (Villaver et al. 2004). The cluster's known distance and reddening allow the determination of the mass and spectral type of the hypothetical companion (assuming that it is on the MS), from the cluster's theoretical subsolar isochrone adopted in Section 2.2 and its estimated visual magnitude (see De Marco et al. 2013, their table C1). Consequently, following the same steps as in Section 3.1, we calculated the new candidate CSPN visual magnitudes, effective temperatures, luminosities and masses, which are presented along with the corresponding derived companion masses and spectral types in Table 5. The quoted CSPN visual magnitudes, luminosities

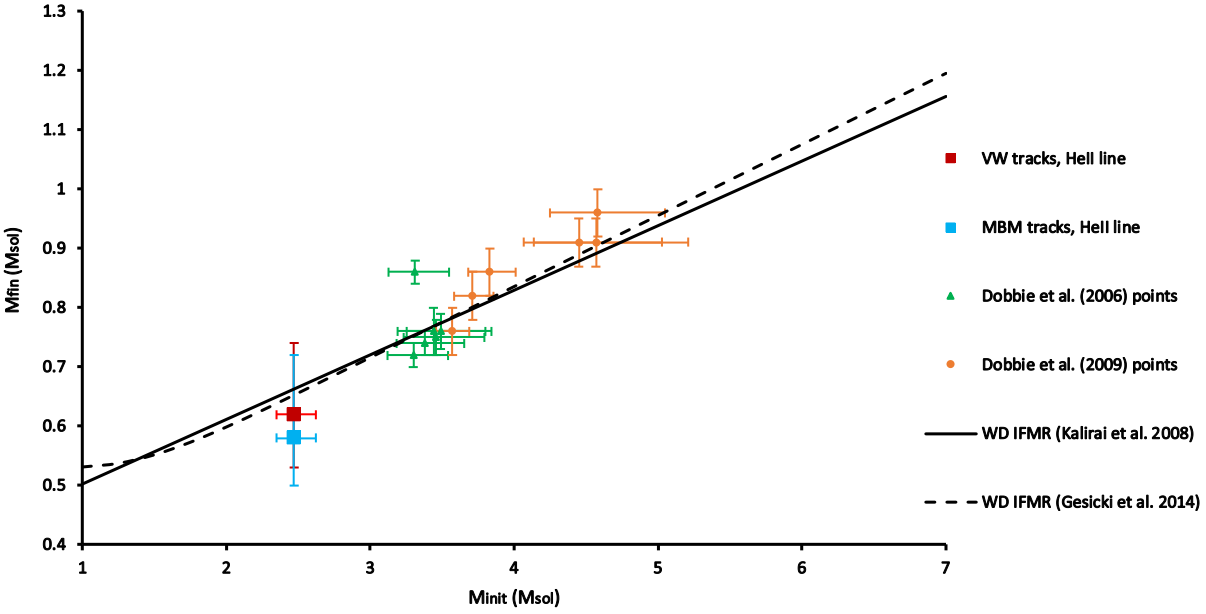

Figure 10. The central star's computed initial (from the cluster's colour–magnitude diagram) and final (from both the VW and the MBM tracks) mass plotted together with the initial and final mass points from Dobbie et al. (2006, 2009) and the Kalirai et al. (2008) and Gesicki et al. (2014) initial-to-final mass relationship. The initial-mass error bars reflect the errors in the derived cluster parameters.

and masses were computed from the $T_{\rm He}$ (c.f. Section 3.3.6) and either the H- or the He-burning evolutionary tracks (depending on their proximity to the CS points), but no masses were estimated for CSPN parameters that fall far from the evolutionary tracks as they are not reliable. The new CSPN physical parameters plotted in the log T–log L plane along with their initial estimates (assuming that 100 per cent of the flux comes from the CSPN) and the subsolar metallicity evolutionary tracks from Vassiliadis & Wood (1994) and Miller Bertolami (2016) are shown in Fig. 9.

Assuming that no significant mass transfer occurs between the two components of a binary system, their mass difference should be large enough to allow the more massive star to evolve as a PN first (see Villaver et al. 2004), a condition that is satisfied in all the cases explored here, where the possible companion is a K dwarf. The PN distance implies that a supergiant companion cannot be justified from the measured visual fluxes, and giant and subdwarf O companions are unlikely owing to their short lifetimes (Renzini & Buzzoni 1986; Yungelson, Tutukov & Livio 1993) and the short time-scales during which they produce significant visual light (see Villaver et al. 2004), respectively. However, a MS, subdwarf or red dwarf companion is still a possibility. From Fig. 9, it can be seen that a flux contribution of more than 50 per cent from a companion would result in a progenitor mass much larger than the cluster's TO mass of $\sim$2.2 $M_{\odot}$, so we can safely rule out this possibility. However, a companion contribution of $\leq$ 50 per cent to the total observed visual flux results in progenitor masses close to 2.2 $M_{\odot}$, within the errors, and thus such a case should be explored further.

Our precisely measured F814W magnitude provides hints regarding the possibility of the presence of an unresolved cool, low-mass companion, because a CSPN is expected to radiate primarily at UV and blue wavelengths, and the companion will yield an infrared (IR) excess (see Moreno-Ibánez et al. 2016; Barker et al. 2018). The observed IR excess is not, however, a definitive indication of a cooler companion but could instead imply an unusual stellar atmosphere or inaccurate reddening estimates (see Barker et al. 2018). Using the IRAF/STSDAS SYNPHOT package (see Section 3.1.3), we used blackbody models and found the expected F555W − F814W colour for a CSPN temperature equal to that derived before assuming zero contribution from a companion. The adopted temperature value of 112 680 K reflects our yields of $T_{\rm He}$. Any (reasonable for a CSPN) value would not significantly change our results. We compared the modelled colours to our measured reddened F555W − F814W colours, and these are presented along with their differences in Table 6. As can be seen, our CSPN presents no IR excess, although the magnitude errors are quite large. This suggests that the presence of a cool companion is unlikely but cannot be excluded. Similarly, we calculated the expected F200LP − F350LP colour (presented in Table 6, along with its difference from our measured value), showing that the measured near-UV colour agrees, within the errors, with that expected for a CSPN of the derived temperature.

4 DISCUSSION

Our new CMD provided by *HST* data is a significant improvement on what was previously available for this cluster. It confirms previous studies that show that AL 1 is an intermediate-age, distant, highly reddened OC. A solar metallicity would not explain the high N/O abundance ratio of 0.87 present in the PN (see Parker et al. 2011), as the latest AGB models (Karakas 2010; Karakas & Lugaro 2016; Ventura et al. 2018) predict that, in solar metallicity environments, such high N abundances cannot result from such low-mass stars. The adopted cluster metallicity of $Z = 0.006$ marginally agrees with the latest predictions of AGB yields (Karakas & Lugaro 2016) for the derived TO mass of $\sim$2.2 $M_{\odot}$. Precise abundance studies will be required to clarify this issue, but these are beyond the scope of this paper.

Our deep *HST* F200LP and F350LP filter images reveal that the nebular core is a faint blue star close to the centre of the bipolar waist (see Fig. 8). It is unlikely that any other star could be the central star of the detected PN, as it would either be unusually red or fall

too far from the well-resolved apparent nebular centre. It is also unlikely for an even fainter CSPN not to be visible at the defined distance with the depth achieved here, of $V = 26$ mag, unless it was a member of an unresolved binary system with a much brighter companion or hidden by a foreground star. This can be excluded based on our near-UV data, at least in the proximity of the nebular centre. An object fainter than $V = 26$ would be either much further than the cluster's adopted distance or unreasonably hot for a CSPN.

Our results indicate that the true core of PHR 1315 − 6555 is a faint CSPN, whose estimated parameters agree, within the errors, with the cluster TO mass and result in a PN core mass of about 0.62 $M_\odot$ from the VW tracks and of about 0.58 $M_\odot$ from the new, faster, MBM tracks. This is about average for a Galactic CSPN (see Moreno-Ibánez et al. 2016) and consistent with what is expected for a Type I PN originating from a higher-mass progenitor of ∼2.2 $M_\odot$. The estimated effective temperature is still much lower than predicted from the crossover method (209×10^3 K) and the excitation class parameter (265×10^3 K, see Parker et al. 2011), but considering that both of these methods give just an approximation of the true effective temperatures our direct measurements supersedes these estimations.

Theoretical cluster isochrones (Girardi et al. 2000; Bressan et al. 2012; Marigo et al. 2017) for the derived cluster parameters predict that the progenitor mass of post-AGB stars is about 2.47 $M_\odot$. The initial and the remnant mass of our CSPN provide a unique additional point for the IFMR from WD studies. Fig. 10 shows our results from both the VW and the MBM tracks plotted along the initial and final mass points from Dobbie et al. (2006, 2009) and the WD IFMR from Kalirai et al. (2008) and Gesicki et al. (2014). As can be seen, the final mass calculated from the VW tracks better fits their data.

The calculated PN intrinsic radius of ∼0.42 pc confirms the nebular evolved nature (Frew & Parker 2010; Parker et al. 2011), and for a typical mean expansion velocity of 24 km s^{-1} (Frew 2008) its age is estimated to be about 17 000 yr. The estimated nebular age also agrees within the errors with that predicted from the MBM tracks for a CS of the derived mass. The newly derived parameters for the PN distance and angular radius, and assuming a canonical spherical shape, a filling factor $\varepsilon = 1$ and the Hβ flux as in Parker et al. (2011), yield a PN ionized mass of ∼0.23 $M_\odot$ (see Pottasch 1996). The relatively low CS luminosity confirms that it is an evolved CSPN, in agreement with the evolved PN nature, and consistent with the fast evolution of a high-mass progenitor (see Villaver et al. 2003).

The apparent absence of a binary companion is controversial for a bipolar nebula (De Marco 2009) such as the one examined here, and this study indicates that extreme shapes may be produced even without any significant contribution from a companion, at least in the case of massive stars.

The integrity of our adopted method for determining the CSPN luminosity and effective temperature rests on the assumptions that the nebula is optically thick and that the nebular internal extinction is negligible.

5 CONCLUSIONS

We have used our deep *HST* photometric data to constrain the physical parameters of the Galactic open cluster AL 1 using the deepest CMD ever constructed for this cluster. Our new results, presented in Table 1, are in close agreement with those from the best previous studies but with tighter errors. We confirm that this intermediate-age cluster is indeed one of the most distant known in our Galaxy. Furthermore, the *HST* data have allowed us to identify for the first time the CSPN of PHR 1315 − 6555, a unique PN proven to be a member of OC AL 1 (Parker et al. 2011). Our analysis indicates that, as might be expected, it is a hot blue star close to the nebular apparent centre. Our findings are of great interest because they uniquely provide direct measurements of the physical parameters of a Galactic CSPN in an OC with a precisely known distance.

ACKNOWLEDGEMENTS

The first author thanks the University of Hong Kong for the provision of a PhD scholarship. The second author acknowledges the support of GRF grants 17326116 and 17300417 from the Research Grants Council of Hong Kong, which helped to make this research possible.

REFERENCES

Allen C. W., 1976, Astrophysical Quantities, Athlone, London
Alonso A., Arribas S., Martinez-Roger C., 1996, A&A, 313, 873
Andrews A. D., Lindsay E. M., 1967, IrAJ, 8, 126
Artusi E., Conselvan G., Tegon A., Zardin D., 2016, JAVSO, 44, 149
Badenes C., Maoz D., Ciardullo R., 2015, ApJ, 804, L25
Barker H. et al., 2017, MNRAS, 475, 4504
Benedict G. F. et al., 2009, AJ, 138, 1969
Blocker T., 1995, A&A, 299, 755
Bonatto C., Bica E., 2011, MNRAS, 415, 2827
Bowen G. H., 1988, ApJ, 329, 299
Bressan A., Marigo P., Girardi L., Salasnich B., Dal Cero C., Rubele S., Nanni A., 2012, MNRAS, 427, 127
Cardelli J. A., Clayton G. C., Mathis J. S., 1989, ApJ, 345, 245
Carraro G., Chiosi C., 1994, A&A, 287, 761
Carraro G., Janes K. A., Eastman J. D., 2005, MNRAS, 364, 179
Carraro G., Munari U., 2004, MNRAS, 347, 625
Carraro G., Vallenari A., Ortolani S., 1995, A&A, 300, 128
Chen Y., Bressan A., Girardi L., Marigo P., Kong X., Lanza A., 2015, MNRAS, 452, 1068
Corradi R. L. M., Schwarz H. E., 1995, A&A, 293, 871
Davis L. E., 1989, A User's Guide to the IRAF Apphot Package. National Optical Astronomy Observatories. Revised May, NOAO, Tucson, Arizona
Davis L. E., 1994, A Reference Guide to the IRAF/DAOPHOT Package, NOAO, Tucson, Arizona
De Marco O., 2009, PASP, 121, 316
De Marco O., Passy J.-C., Frew D. J., Moe M., Jacoby G. H., 2013, MNRAS, 428, 2118
Dobbie P. D., Napiwotzki R., Burleigh M. R., Williams K. A., Sharp R., Barstow M. A., Casewell S. L., Hubeny I., 2009, MNRAS, 395, 2248
Dobbie P. D. et al., 2006, MNRAS, 369, 383
Dressel L., 2012, Wide Field Camera 3 Instrument Handbook for Cycle 21 v.5.0, STScI, Baltimore, MD
Dressel L., 2017, Wide Field Camera 3 Instrument Handbook, Version 9. STScI, Baltimore, MD
Ferrario L., Wickramasinghe D., Liebert J., Williams K. A., 2005, MNRAS, 361, 1131
Flower P. J., 1996, ApJ, 469, 355
Frew D. J., 2008, PhD thesis, Macquire University, Sydney, Australia
Frew D. J., Parker Q. A., 2010, PASA, 27, 129
Frew D. J., Parker Q. A., Bojičić I. S., 2016, MNRAS, 455, 1459
Frinchaboy P. M., Majewski S. R., Crane J. D., Reid I. N., Rocha-Pinto H. J., Phelps R. L., Patterson R. J., Muñoz R. R., 2004b, ApJ, 602, L21
Frinchaboy P. M., Munoz R. R., Majewski S. R., Friel E. D., Phelps R. L., Kunkel W. B., 2004a, preprint (astro-ph/0411127)
Gabler R., Kudritzki R. P., Mendez R. H., 1991, A&A, 245, 587
Gaia Collaboration et al., 2016, A&A, 595, A1

García-Segura G., Villaver E., Langer N., Yoon S.-C., Manchado A., 2014, ApJ, 783, 74
Gesicki K., Zijlstra A. A., Hajduk M., Szyszka C., 2014, A&A, 566, A48
Giammanco C. et al., 2011, A&A, 525, A58
Gillett F. C., Jacoby G. H., Joyce R. R., Cohen J. G., Neugebauer G., Soifer B. T., Nakajima T., Matthews K., 1989, ApJ, 338, 862
Girardi L., Bressan A., Bertelli G., Chiosi C., 2000, A&AS, 141, 371
Gleizes F., Acker A., Stenholm B., 1989, A&A, 222, 237
Gruenwald R., Viegas S. M., 2000, ApJ, 543, 889
Gruenwald R., Viegas S. M., 2002, RMxAC, 14, 117
Harman R. F., Seaton M. J., 1966, MNRAS, 132, 15
Herwig F., 2000, A&A, 360, 952
Horne K., 1988, Davis Philip A. G., Donald S. H., Saul J. A., Application of Synthetic Photometry Techniques to Space Telescope Calibration, New Directions in Spectrophotometry, L. Davis Press, Schenectady, N. Y.
Iben I., Jr, 1984, ApJ, 277, 333
Jacoby G. H., Morse J. A., Fullton L. K., Kwitter K. B., Henry R. B. C., 1997, AJ, 114, 2611
Janes K. A., Phelps R. L., 1994, AJ, 108, 1773
Kaler J. B., 1983, ApJ, 271, 188
Kaler J. B., Jacoby G. H., 1989, ApJ, 345, 871
Kaler J. B., Lutz J. H., 1985, PASP, 97, 700
Kalirai J. S., Hansen B. M. S., Kelson D. D., Reitzel D. B., Rich R. M., Richer H. B., 2008, ApJ, 676, 594
Karakas A. I., 2010, MNRAS, 403, 1413
Karakas A. I., Lugaro M., 2016, ApJ, 825, 26
Kimble R. A., MacKenty J. W., O'Connell R. W., Townsend J. A., 2008, SPIE, 7010, 70101E
Koornneef J., Bohlin R., Buser R., Horne K., Turnshek D., 1986, HiA, 7, 833
Laidler V. et al., 2005, Synphot User's Guide, Version 5.0. STScI, Baltimore, MD
Lauberts A., 1982, ESO/Uppsala survey of the ESO(B) atlas, ESO, Garching
Luridiana V., Morisset C., Shaw R. A., 2015, A&A, 573, A42
Majaess D., Carraro G., Moni Bidin C., Bonatto C., Turner D., Moyano M., Berdnikov L., Giorgi E., 2014, A&A, 567, A1
Majaess D. J., Turner D. G., Lane D. J., 2007, PASP, 119, 1349
Majaess D. J., Turner D. G., Lane D. J., Krajci T., 2011, JAVSO, 39, 219
Manchado A., Villaver E., Stanghellini L., Guerrero M. A., 2000, in Kastner J. H., Soker N., Rappaport S., eds, Asymmetrical Planetary Nebulae II: From Origins to Microstructures, ASP Conference Series, Vol. 199, San Francisco
Marigo P., Girardi L., 2007, A&A, 469, 239
Marigo P. et al., 2017, ApJ, 835, 77
Miller Bertolami M. M., 2016, A&A, 588, A25
Moni Bidin C. et al., 2014, A&A, 561, A119
Moreno-Ibáñez M., Villaver E., Shaw R. A., Stanghellini L., 2016, A&A, 593, A29
Neckel T., Klare G., 1980, A&AS, 42, 251
Osterbrock D. E., Ferland G. J., 2006, Astrophysics of Gaseous Nebulae and Active Galactic Nuclei. University Science Books, Sausalito, CA
Parker Q. A., Frew D. J., Miszalski B., Kovacevic A. V., Frinchaboy P. M., Dobbie P. D., Köppen J., 2011, MNRAS, 413, 1835
Parker Q. A. et al., 2005, MNRAS, 362, 689
Parker Q. A. et al., 2006, MNRAS, 373, 79
Pease F. G., 1928, PASP, 40, 342
Peimbert M., 1978, IAUS, 76, 215
Peimbert M., Torres-Peimbert S., 1983, in Flower D. R., ed., Proc. IAU Symp. 103. Kluwer, Dordrecht, p. 233
Perinotto M., Schönberner D., Steffen M., Calonaci C., 2004, A&A, 414, 993
Perren G. I., Vázquez R. A., Piatti A. E., 2015, A&A, 576, A6
Phelps R. L., Janes K. A., Montgomery K. A., 1994, AJ, 107, 1079
Pottasch S. R., 1996, A&A, 307, 561
Preite-Martinez A., Pottasch S. R., 1983, A&A, 126, 31
Rajan A. et al., 2011, WFC3 Data Handbook v.2.1, STScI, Maryland
Reid W. A., Parker Q. A., 2010, PASA, 27, 187
Renzini A., 1989, IAUS, 131, 391
Renzini A., Buzzoni A., 1986, ASSL, 122, 195
Sabbi E., Bellini A., 2013, UVIS PSF Spatial & Temporal Variations. STScI, Maryland
Schönberner D., 1983, ApJ, 272, 708
Schönberner D., 1986, A&A, 169, 189
Shaw R. A., 2006, IAUS, 234, 305
Shaw R. A., Kaler J. B., 1985, ApJ, 295, 537
Shaw R. A., Kaler J. B., 1989, ApJS, 69, 495
Stanghellini L., Shaw R. A., Villaver E., 2008, ApJ, 689, 194–202
Stanghellini L., Shaw R. A., Villaver E., 2016, ApJ, 830, 33
Stanghellini L., Villaver E., Manchado A., Guerrero M. A., 2002, ApJ, 576, 285
Stetson P. B., 1987, PASP, 99, 191
Turner D. G., Rosvick J. M., Balam D. D., Henden A. A., Majaess D. J., Lane D. J., 2011, PASP, 123, 1249
Tylenda R., Acker A., Gleizes F., Stenholm B., 1989, A&AS, 77, 39
Vacca W. D., Garmany C. D., Shull J. M., 1996, ApJ, 460, 914
van den Bergh S., Hagen G. L., 1975, AJ, 80, 11
Vassiliadis E., Wood P. R., 1994, ApJS, 92, 125
Ventura P., Karakas A., Dell'Agli F., García-Hernández D. A., Guzman-Ramirez L., 2018, MNRAS, 475, 2282
Villaver E., Manchado A., García-Segura G., 2002, ApJ, 581, 1204
Villaver E., Stanghellini L., Shaw R. A., 2003, ApJ, 597, 298
Villaver E., Stanghellini L., Shaw R. A., 2004, ApJ, 614, 716
Villaver E., Stanghellini L., Shaw R. A., 2007, ApJ, 656, 831
Weidemann V., 1987, A&A, 188, 74
Willson L. A., 2000, ARA&A, 38, 573
Willson L. A., Bowen G. H., Struck C., 1996, ASPC, 98, 197
Wood P. R., 1979, ApJ, 227, 220
Wood P. R., Faulkner D. J., 1986, ApJ, 307, 659
Yungelson L. R., Tutukov A. V., Livio M., 1993, ApJ, 418, 794
Zanstra H., 1931, ZA, 2, 1

This paper has been typeset from a TEX/LATEX file prepared by the author.